Ahmed A. Abdulshaheed
Department of Mechanical Engineering,
University of South Carolina,
Columbia, SC 29208
e-mail: abdulsha@email.sc.edu

Pengtao Wang
Department of Mechanical Engineering,
University of South Carolina,
Columbia, SC 29208
e-mail: pwnnx@Missouri.edu

Guanghan Huang
Department of Mechanical Engineering,
University of South Carolina,
Columbia, SC 29208
e-mail: huanggu@email.sc.edu

Yueyang Zhao
Department of Mechanical Engineering,
University of South Carolina,
Columbia, SC 29208
e-mail: yueyang@email.sc.edu

Chen Li[1]
Department of Mechanical Engineering,
University of South Carolina,
Columbia, SC 29208
e-mail: li01@cec.sc.edu

Filling Ratio Optimization for High-Performance Nanoengineered Copper-Water Heat Pipes

This experimental test investigates the effect of filling ratio (FR) and inclination angle on the thermal performance of a nanoengineered copper-water heat pipe. A hydrophilic copper oxide coating (CuO) is synthesized and integrated on the inner wall of the evaporation section of the heat pipe. The heat pipe is fabricated from an inner grooved copper pipe with dimensions of 12.7 mm outer diameter, 11 mm inner diameter, and 440 mm length. Ultra-filtered de-ionized (DI) water is used as a working fluid. Four different FRs of DI water 3%, 5%, 10%, and 15% are investigated to determine the optimum configuration. All samples are tested at various inclination angles and working loads. Experimental results show that the optimum filling ratio is the 5% FR, which was indicated by the lowest thermal resistance of 0.019 K/W. [DOI: 10.1115/1.4050225]

Keywords: nanoengineered coating, copper oxide CuO, filling ratio, grooved copper heat pipe, condensation, evaporation, heat pipes

1 Introduction

A heat pipe is a passive heat transfer device that consists of a hermetically sealed vessel charged with a working fluid after being vacuumed. A heat pipe transfers heat from one end to another at a small temperature difference by implementing the working fluid phase change process. Unique characteristics of heat pipes such as low thermal resistance, simple fabrication process, and zero external-energy requirements for operations have contributed to the widespread use of the heat pipe in many applications, including heat exchangers [1], A/C systems [2], electronics cooling [3–5], and solar collectors [6,7]. Generally, evaporation, adiabatic, and condensation sections are the main functional parts of any heat pipes. As the heat is being applied to the evaporation section, the working fluid absorbs that heat through latent heat vaporization. Due to pressure difference, this vapor flows from the evaporation section through the adiabatic section to reach the condensation section, where the vapor releases the heat to the walls through condensation. This heat transfer cycle ends with the return of the condensate with the help of capillary forces and gravity to the evaporation section. The working fluid phase change process involves a large amount of latent heat such that a considerable amount of heat can be transferred with a small temperature difference between evaporation and condensation sections [8], which leads to extremely high effective thermal conductivity of small thermal resistance.

As it has a predominant effect on a heat pipe's thermal performance, filling ratio (FR) has been extensively studied by researchers. For example, Lips et al. [9] experimentally investigated and visualized the effect of filling ratio on a flat plate heat pipe with inner grooves. The visualization study showed that the evaporator experiences a partially dry out at a small filling ratio. While at high filling ratios, the condenser section is flooded. Five different filling ratios were studied. The results showed the significant influence of the filling ratio on the heat pipe performance. They concluded that the optimum filling ratio is about 1–2.5 times the groove's total volume. Subsequently, Senthil et al. [10] investigated four different filling ratios of Al_2O_3 nanofluid on a cylindrical copper heat pipe's thermal performance. A 66% enhancement of thermal efficiency was reached by charging 75% of the evaporator volume working fluid. While for the inclination angle, 30 deg showed the best performance. Chen and Chou [11] examined the steady-state conditions of a flat heat pipe to determine the optimum filling ratio. The working fluid was acetone. Ten filling ratios were tested. Results showed that a 25% filling ratio (of evaporator volume) gave the best performance, where a maximum heat transport capability of 47 W was recorded. Also, the lowest thermal resistance achieved was 0.254 K/W, and the highest thermal conductivity was 3150 W/(m K). Tharayil et al. [12] investigated the effect of the filling ratio on a miniature loop heat pipe. Three filling ratios were used: 20%, 30%, and 50% of the evaporator's volume. The study confirmed the significant effect of filling ratio on the heat pipe's thermal performance. For a heat input range of 20–380 W, the results showed that the 30% filling ratio provided the best performance, with a low thermal resistance of 0.106 K/W. Sukchana and Jaiboonma [13] used three different filling ratios: 10%, 15%, and 20% of evaporator's volume and three different adiabatic lengths: 300, 500, and 700 mm to study and compare the effect of adiabatic length and filling ratio on a long heat pipe's thermal performance. They concluded that the filling ratio has more impact on the performance compared with the adiabatic length. Furthermore, the optimum filling ratio was 15% for all lengths of the adiabatic section. An internally finned heat pipe was tested by Naresh and Balaji [14] to investigate the effect of filling ratio on the performance. Three filling ratios were used: 20%, 50%, and 80% of the evaporator's volume and two working

[1]Corresponding author.

Manuscript received May 21, 2020; final manuscript received January 31, 2021; published online March 30, 2021. Assoc. Editor: Arvind Narayanaswamy.

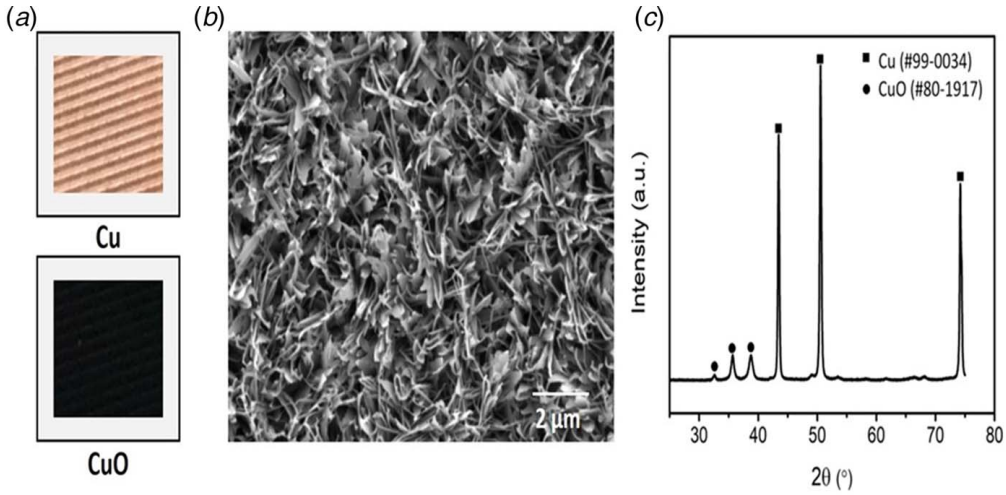

Fig. 1 Surface morphology and components of surface coatings: (*a*) image of surface before and after oxidization, (*b*) SEM image, and (*c*) XRD patterns of prepared CuO nanostructures [22]

fluids: water and acetone. The experimental results showed that the 50% filling ratio provided the best thermal performance for both working fluids, while the other two filling ratios went through dry out and flooding conditions. A model to study the evaporator wettability was done by Xu et al. [15] and compared with their experimental results. Hydrophilic and hydrophobic surfaces were compared. Also, three filling ratio conditions were investigated: a low filling ratio (<20%), a regular filling ratio (20–30%), and a high filling ratio (>30%). The optimum filling ratio in their tests was in the range of 20–30%. Results also showed poor thermal performance of the hydrophobic surface compared with the hydrophilic one. The impact of filling ratio ranging between 25% and 98% was investigated by Lv et al. [16]. The tested thermosyphon has a superhydrophilic evaporator and slippery lubricant-infused porous condenser. The results indicated that the filling ratio strongly influenced the overall heat transfer performance. At a filling ratio of 25%, the film evaporation heat transfer was dominant. Meanwhile, at 98%, the pool boiling was the dominant heat transfer mechanism. So, the 40% filling ratio showed optimum results for all tests. Alammar et al. [17] implemented a two-phase CFD simulation to study the effect of filling ratio and inclination angle on a thermosyphon's thermal performance. Five filling ratios: 25%, 35%, 65%, 80%, and 100% of the evaporator's volume and five inclination angles: 10 deg, 30 deg, 50 deg, 70 deg, and 90 deg were considered. The results showed that a 65% filling ratio and a 90 deg inclination angle exhibited the best thermal performance. Another simulation was done by Shabgard et al. [18], where the effect of filling ratio on the transient performance of a vertical thermosyphon was studied. They indicated that short thermal response time and lowest thermal resistance conveyed an optimum filled thermosyphon. They recommended adding an extra small amount of working fluid to the optimum filling ratio to avoid the dry out that could happen with heat input fluctuations. Aly et al. [19] investigated the effect of four filling ratios: 20%, 40%, 60%, and 80% of the evaporator volume and four inclination angles: 0 deg, 30 deg, 60 deg, and 90 deg experimentally. A helically micro-grooved heat pipe with water-based alumina nanofluid was implemented. They achieved an 18.2% reduction in thermal resistance with an inclination angle of 60 deg and a filling ratio of 80%. They titled the 60 deg inclination angle and 80% filling ratio as the optimum conditions for their test. Another investigation was conducted by Jafari et al. [20] to test a thermosyphon with five different filling ratios: 8%, 16%, 35%, 50%, and 100% of the evaporator's volume with a heat load ranging from 30 to 900 W. The thermosyphon's inner diameter was 33 mm, and water was the working fluid. The optimum performance achieved was at a filling ratio of 35%. At lower filling ratio, dry out happens at high heat inputs. While for the 100% filling ratio, the thermosyphon went through the pool boiling process. The experimental results showed a good agreement with other correlations in the same area of interest. Finally, Sarafraz et al. [21] implemented a wickless thermosyphon charged with a biologically produced eco-friendly working fluid to investigate the effect of the filling ratio and the inclination angle. Among six filling ratios and five inclination angles, the results showed that the optimum thermal performance was achieved with a 0.65 filling ratio and 55 deg inclination angle.

This experimental work seeks to fill in the gap noticed in the literature above in the manner of producing a high thermal conductivity heat pipe and implementing nanoengineered coating. The experimental work will start by synthesizing and integrating the nanoengineered hydrophilic coating, nanostructure (CuO). This nanostructure was experimentally tested in our previous published work [22] and proved to highly enhance the heat pipe performance compared with another type of coating and a bare heat pipe. Afterward, investigating the effect of four FRs, FR being defined as the volume of the working fluid to the evaporation section volume, on the nanoengineered hydrophilic coated heat pipe. Furthermore, the impact of different inclinations and heat loads was investigated. Heat pipes have been fabricated and systematically characterized in this research.

2 Experimental Part

2.1 CuO Nanostructure Coating Fabrication Process. The CuO nanostructures were directly synthesized on the inner surface of the copper pipe via a wet chemical process. The alkaline solution was prepared with $NaClO_2$ (0.40 M), NaOH (1.25 M), $Na_3PO_4{\cdot}12H_2O$ (0.25 M), and distilled water [23,24]. After precleaning to remove grease contamination and native oxide layer, the copper pipes were immersed in the prepared solution and maintained at 95 °C for 20 min. The prepared sample has spike-like CuO nanostructures (black) with a height of approximately 1 μm, as observed by scanning electron microscopy (SEM; Zeiss Ultra Plus FESEM) (Figs. 1(*a*) and 1(*b*)). X-ray diffraction (XRD) confirms the formation of CuO (using Rigaku MiniFlex II desktop X-ray Diffractometer). The CuO peaks were identified from XRD patterns (PDF#80-1917, marked with • in Fig. 1(*c*)).

2.2 Fabrication of Heat Pipe. The heat pipe samples are manufactured using a grooved copper pipe with parameters and dimensions listed in Table 1 and shown in Fig. 2 [22]. Swagelok vacuum

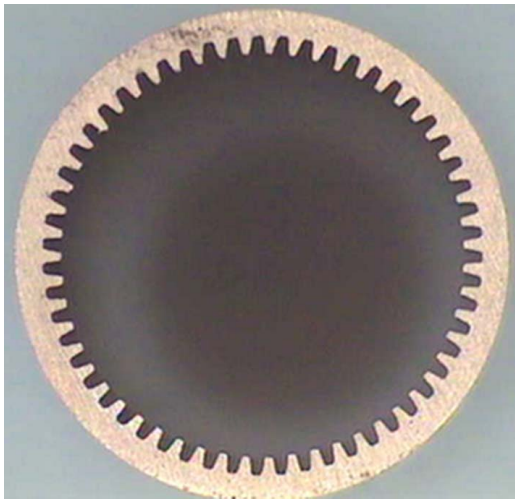

Fig. 2 Inner grooves

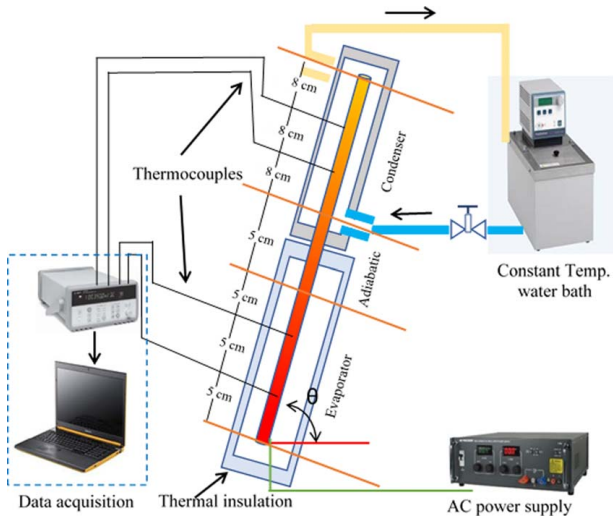

Fig. 3 Schematic diagram of the experimental setup and thermocouple distribution

Table 1 Parameters of the heat pipe [22]

Parameters	Value/material
Tube material	Copper
Working fluid	DI water
Pipe length	440 mm
Outer diameter	12.7 mm
Inner diameter	11 mm
Groove depth	0.28 mm
Number of grooves	75

fittings are used to seal heat pipe ends. All the fittings, pipes, and connections are chemically cleaned to remove all manufacturing oil and contaminations. The evaporation section, with 15 cm length, is fabricated with a nanoengineered, nanostructure, hydrophilic copper oxide coating CuO. The hydrophilic coating is integrated on the heat pipe surface by a hot alkali exposure process, after which the parts are assembled into a heat pipe. The assembled heat pipe is connected to a vacuuming and charging system. Next, a second vacuum process is conducted to remove the non-condensable gases that might be produced during the vacuuming and charging process [25,26].

2.3 Test Setup and Procedure. The test setup used for this research consists of three main parts: cooling chamber, heating chamber, and the inclination mechanism, as shown in Fig. 3. For the cooling chamber, a water jacket, 4″ in diameter, made of a cylindrical tube is used for cooling water circulation around the 24 cm long condenser section of the heat pipe. A constant temperature water bath (RTE-4DD; Neslab) is used to supply the cooling water at a 1.5 l/min flowrate and 35 °C. While for the heating chamber, two aluminum plates (15 cm × 5 cm × 1 cm) are used to cover the evaporation part of the heat pipe. Each plate has four cartridge heaters inserted inside. These heaters are connected to a D.C. power supply, where the power input can be adjusted through the measurement of voltage and current. For the inclination mechanism, the test setup was designed with a hinge such that the inclination angle can freely range from 0 deg to 90 deg. To present and compare the test results, the outer wall temperatures of the heat pipe are measured and recorded by using eight K-type thermocouples. Thermocouples are mounted in four different locations, as shown in Fig. 3, not to scale, two locations on the evaporation section, and another two on the condensation section. Thermal grease is applied to all contact surfaces to enhance the reading ability of the thermocouples. The whole setup is thermally insulated to minimize the amount of heat loss.

3 Data Reduction

In order to measure, compare, and characterize the heat pipe performance, the equations below are implemented. The actual heat input to the heat pipe can be calculated using Eq. (1):

$$Q = I \times V - Q_{loss} \tag{1}$$

where I is the current and V is the voltage supplied to the heaters by the D.C. power supply. While the heat loss is represented in Eq. (2):

$$Q_{loss} = h_{ins} A_{ins} \left(\frac{T_{s1} + T_{s2}}{2} - T_a \right) \tag{2}$$

such that

$$h_{ins} = 3.226 \ln (T_s - T_a) - 0.86 \tag{3}$$

Equation (3) is a semi-empirical formula from our experimental data [22]. Equation (4) is used to calculate the heat flux:

$$q = \frac{Q}{\pi d_o L_e} \tag{4}$$

Equation (5) calculates the total thermal resistance, which is the resistance imposed by the heat pipe against the heat flow from the evaporator to the condenser:

$$R_t = \frac{T_e - T_c}{Q} \tag{5}$$

where T_e and T_c represent the average temperature measured at the evaporation and condensation sections, respectively. The effective thermal conductivity is calculated using Eq. (6) to evaluate the heat pipe's thermal efficiency:

$$k_{eff} = \frac{L_{eff}}{A \times R} \tag{6}$$

where

$$L_{eff} = L - (L_e + L_c)/2 \tag{7}$$

The inside wall temperatures of heat pipe walls are calculated as

$$T_{e,i} = T_e - \frac{Q}{2\pi k_{cop} L_e} \ln\left(\frac{d_o}{d_i}\right) \tag{8}$$

$$T_{c,i} = T_c + \frac{Q}{2\pi k_{cop} L_c} \ln\left(\frac{d_o}{d_i}\right) \tag{9}$$

where $T_{e,i}$ and $T_{c,i}$ are the average inner temperatures of the evaporator and condenser, respectively. L_e and L_c represent the evaporator and condenser length, respectively. The heat transfer coefficient (HTC) is calculated for the evaporator and condenser using Eqs. (10) and (11), respectively:

$$h_e = \frac{Q}{\pi d_i L_e (T_{e,i} - T_v)} \tag{10}$$

$$h_c = \frac{Q}{\pi d_i L_c (T_v - T_{c,i})} \tag{11}$$

where T_v is the vapor temperature, which is equal to the adiabatic wall temperature of the heat pipe. Also, T_v is taken to be equal to T_{sat}, the saturation temperature at P_{sat}, which also is the temperature at which the physical properties of the heat pipe wall materials were determined for theoretical calculations.

In order to validate and compare the experimental results and show the enhancement obtained, Imura boiling heat transfer correlation [20,27] and Nusselt film condensation [28] are used to calculate the HTC theoretically. Imura correlation is presented as

$$h_{e,th} = 0.32\left[\frac{\rho_l^{0.65} k_l^{0.3} Cp_l^{0.7} g^{0.2} Q^{0.4}}{\rho_v^{0.25} H_{fg}^{0.4} \mu_l^{0.1}}\right]\left(\frac{P_{sat}}{P_{amb}}\right)^{0.3} \tag{12}$$

where ρ_l, k_l, Cp_l, and μ_l are the density, thermal conductivity, specific heat capacity, and dynamic viscosity of the working fluid, respectively. ρ_v is the vapor density, H_{fg} is the latent heat of phase change, and P_{sat} and P_{amb} are the saturation pressure of the heat pipe and the ambient pressure, respectively.

While Nusselt correlation is

$$h_{c,th} = 0.943\left\{\frac{g\rho_l^2 k_l^3 [H_{fg} + 0.68 Cp_l (T_{sat} - T_{c,i})]}{\mu_l L_{eff} (T_{sat} - T_{c,i})}\right\}^{0.25} \tag{13}$$

The thermophysical properties of the working fluid are obtained based on the NIST database according to the saturation pressure.

4 Uncertainty Analysis

There are some uncertainties involved in every experimental research. These uncertainties may result from the calibration of instruments, manufacturer's specifications, calibration certificates, and uncertainties assigned in the reference book. For this experiment, measuring parameters like voltage and current are associated with some uncertainties; the thermocouple reading is also of some uncertainty value. The following equation is used to calculate uncertainty [29]. Table 2 indicates the uncertainties associated with the instruments used in this work and the calculated power uncertainty. The details of the uncertainty analysis are given in Ref. [22]

Table 2 Accuracy and uncertainty of measuring instrument and power

Quantity measured	Uncertainty	Unit
Temperature	±0.1	°C
Voltage	±0.2	V
Current	±0.2	A
Power	±0.8	%
HTC_e	±0.9	%
HTC_c	±1.1	%

$$\sigma_p = \pm\sqrt{\left(\frac{\partial p}{\partial I}\sigma_I\right)^2 + \left(\frac{\partial p}{\partial V}\sigma_V\right)^2} \tag{14}$$

5 Results and Discussion

5.1 Effect of Filling Ratio

5.1.1 Temperature Distribution Analysis. Typically, an approximation of the amount of liquid required inside the heat pipe can be achieved by measuring the volume occupied by the wick structure [30,31]. Meanwhile, in this work, applying hydrophilic coating will enhance the surface's wettability, which diverts these calculations from the correct estimation of the filling ratio required for such heat pipes. Thus, the working fluid filling ratio in this study is presented

$$FR = \frac{V_f}{V_e} \times 100\% \tag{15}$$

where FR is the filling ratio, V_f is the working fluid volume, and V_e is the evaporation section volume. Figure 4 shows a typical example of external wall temperature distributions along the heat pipe at a 25 deg inclination angle for four filling ratios under steady-state operating conditions. Figures 4(*a*)–4(*d*) represent the FR of 3%, 5%, 10%, and 15%, respectively. It shows that as the heat input increases, the temperature of all points of the heat pipe increases too. This applies to all the filling ratios used. In Fig. 4(*a*), 3% FR shares a similar temperature trend at low heat inputs compared with the other filling ratios, which is represented by having a low-temperature gradient between the evaporation and the condensation sections. The evaporator temperature started to rise dramatically after 90 W, going into 120 W, leading to dry out conditions at 150 W. When the filling ratio is smaller than the optimal filling ratio, dry areas will present at the evaporation section (no liquid film cover), especially at high heat inputs where higher evaporation rate occurs. Consequently, the sample will experience a rapid rise in the wall temperature leading to performance degradation [32]. In Fig. 4(*b*), 5% FR shows the smoothest and the most uniform temperature profile among all the other figures. The 5% FR showed the smallest temperature difference between heat pipe ends. The temperature difference measured for the 5% FR is ranging from 1 °C at 30 W to 3 °C at 150 W. As with all other figures, for this case, the temperature of all points increased as the heat input increased. Yet, it was the flattest profile with almost no slope between the evaporator and condenser temperatures. From Figs. 4(*a*)–4(*d*) by comparing the temperature differences on the heat pipe ends, it can be concluded that Fig. 4(*b*) (i.e., 5% FR) represents the optimum filling ratio for such heat pipe configuration under such working conditions. The highest temperature difference occurred for the 3% FR was 3.1 °C, while it was 5.1 °C for Figs. 4(*c*) and 4(*d*). This conclusion is drawn from the flat temperature profile and the low-temperature difference throughout all cases compared with the other filling ratios. For the filling ratio of 10%, Fig. 4(*c*), the temperature gradient for the 30 W is similar to Fig. 4(*b*). Meanwhile, the temperature gradient started to increase as the heat input increased beyond 30 W. The evaporator temperature of Fig. 4(*c*) is higher than that of Fig. 4(*b*) for most cases. This is due to the presence of a liquid pool at the evaporation section as the working fluid amount is larger compared with Fig. 4(*b*) [28]. The highest temperature difference reached for this case was 5.1 °C. Figure 4(*d*) explicitly clarifies the effect of overfilling the heat pipe, where the evaporator temperature is remarkably higher than the evaporator temperature of Fig. 4(*b*). Whereas Figs. 4(*c*) and 4(*d*) represent the overfilled conditions where the heat pipe has a large amount of working fluid, once again, the temperature difference was 5.1 °C. The abundance of the working fluid will form a liquid

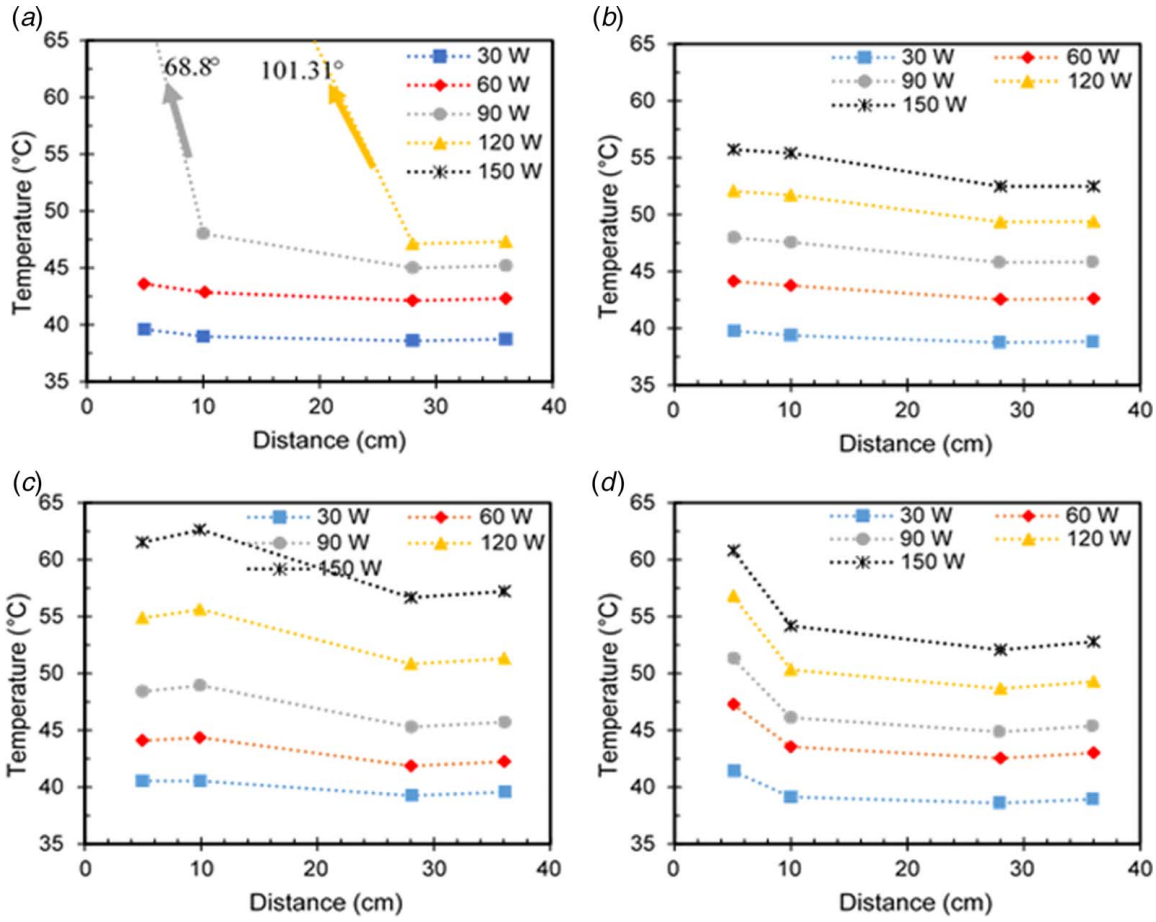

Fig. 4 Axial temperature distribution for 25 deg inclination angle: (*a*) FR = 3%, (*b*) FR = 5%, (*c*) FR = 10%, and (*d*) FR = 15%

pool at the evaporation section which will make the convection heat transfer mechanism the predominant way. For optimum filling ratio, i.e., Fig. 4(*b*), having an adequate amount of working fluid will form a thin liquid film on the evaporation section's inner walls. As it has higher thermal transfer abilities over convection, the thin liquid film will augment the overall thermal performance of the heat pipe [18,33].

5.1.2 Evaporation Heat Transfer. Multiple and diverse heat transfer processes occur in the evaporation section of a heat pipe, including thin film evaporation, pool boiling, convection, and sometimes a mixture of two or more of these processes at the same time. Previously mentioned, Eq. (12) represents a correlation developed by Imura et al. [27] to calculate the heat transfer coefficient at the evaporator of a thermosyphon based on nucleate boiling. Figure 5 shows a comparison between the experimental results of the present research and Imura's correlation. Figures 5(*a*)–5(*d*) represent the evaporator HTC with multiple heat fluxes at 25 deg, 55 deg, 75 deg, and 90 deg inclination angle, respectively. Results clearly show that the 3% FR has the highest HTC, but for low heat inputs only, a colossal degradation in terms of HTC occurred when the heat input increased for this case. The second case to discuss is 5% FR. This case has the highest and the steadiest evaporation HTC for all heat input cases. As we expected and mentioned before, the 5% FR case represents the optimum filling ratio in terms of HTC also for this heat pipe. The 10% FR case has a lower HTC than the 5% FR, but still slightly higher than Imura results. The last case is the 15% FR, which was the closest case to Imura results in all figures. This agreement between Imura's predictions and the experimental data of the 15% FR can be explained by the fact that Imura correlation is based on the nucleate boiling, which happens in a liquid pool, thus as mentioned earlier, a liquid pool will be present for the 15% FR case. The same agreement was reported between the Imura correlation and experimental results of Lataoui and Jemni for the overfilled case and related to the corresponding previous reason [33].

5.1.3 Condensation Heat Transfer. Figures 6(*a*)–6(*d*) present both the predicted, using Nussselt correlations, and experimental condensation HTC of the heat pipe. Nusselt correlation, Eq. (12), is used to calculate the condensation HTC theoretically. Formerly shown in Fig. 4, the temperatures at the condensation section of all samples, for all filling ratios, are so close to each other with no noticeable change. This means most enhancement achieved is in the evaporation section, not the condensation section, due to the nanoengineered coating. Figures 6(*a*)–6(*d*) represent the HTC of condensation for four different inclination angles: 25 deg, 55 deg, 75 deg, and 90 deg. Owning a higher volume of condensate, the 15% FR case will lead to a higher shear force acting on the condensate film. Hence, the condensation HTC falls below the Nusslet correlation. It is clear that the condensation HTC is dependent on the heat input, as shown in Figs. 6(*a*)–6(*d*). For example, for the 5% FR in Fig. 6(*a*), the condensation HTC increased from 5 kW/(m^2 K) to 7.5 kW/(m^2 K) when the heat input increased from 30 W to 150 W. The same trend of condensation HTC can be observed for all samples under test conditions. The results indicate that the subcooling degree between the condenser surface and the saturated vapor increases as the heat input increases because of the saturated vapor temperature increases as the pressure of the saturated vapor increase inside the heat pipe [23]. Finally, it is apparent that a small amount of enhancement is obtained in the condensation section as comparing the predicted and experimental condensation

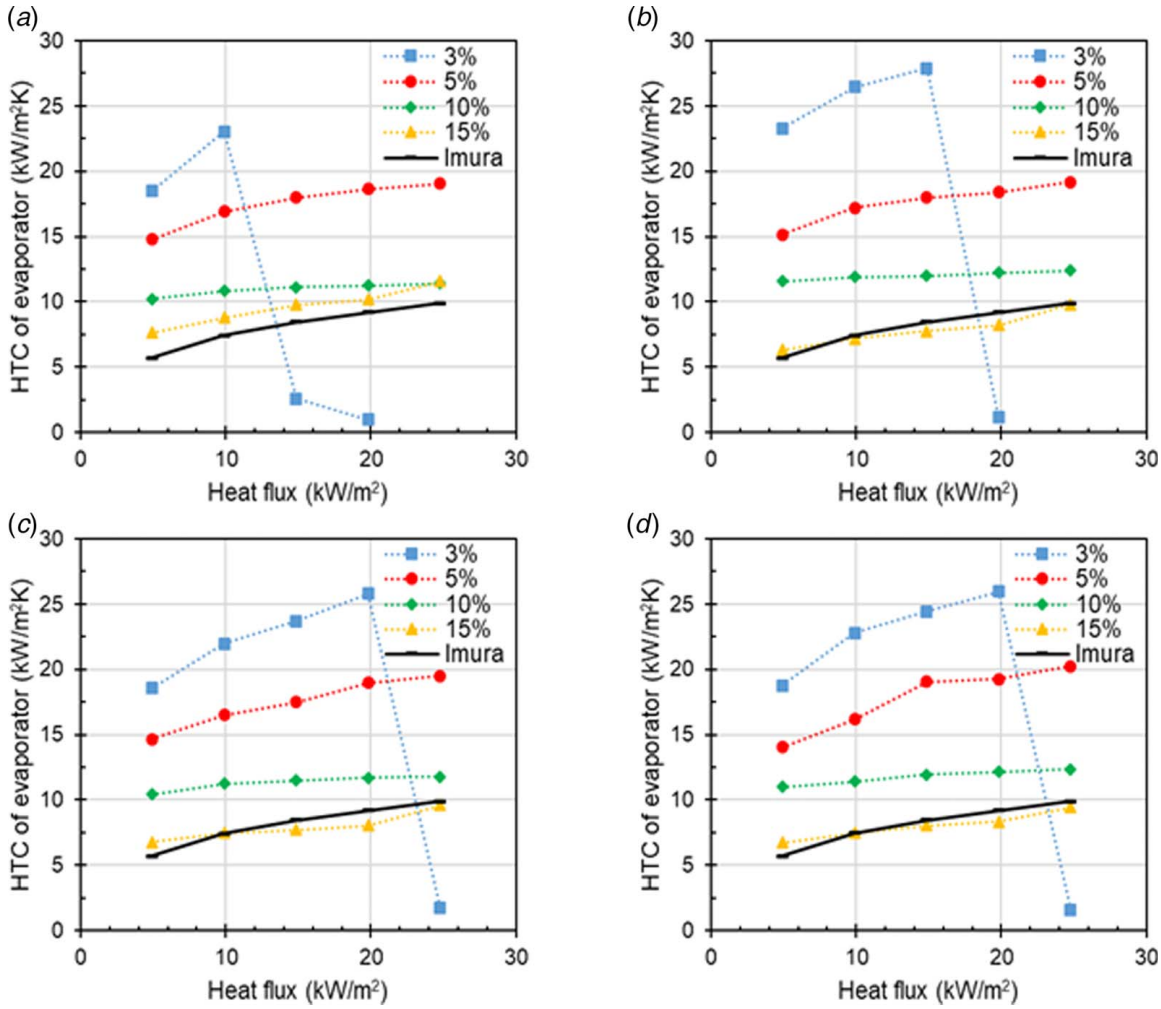

Fig. 5 Predicted and experimental HTC of evaporator for different inclination angles: (*a*) 25 deg, (*b*) 55 deg, (*c*) 75 deg, and (*d*) 90 deg

HTC. If we go back to Figs. 5(*a*)–5(*d*), we can spot the vast enhancement achieved in the evaporator HTC compared with the Imura correlation; once again, this is due to the coating integrated into the evaporation section only in this study.

5.1.4 Thermal Conductivity. To sum up the effect of the filling ratio on the heat pipe thermal performance and clearly determine the optimum conditions, thermal conductivity with heat input is plotted and presented in Fig. 7. Two inclination angles are shown in this figure, 25 deg in Fig. 7(*a*) and 90 deg in Fig. 7(*b*). From looking at Fig. 7(*a*), 25 deg inclination angle case, it can be seen that the 3% FR starts with a high thermal conductivity up to around 120 kW/(m K) then the performance begins to degrade as the heat input increases beyond 60 W leading to dry out conditions at 150 W. This behavior indicates the existence of dry out conditions due to the lack of condensate returning to the evaporation section as the filling ratio is low and limited gravity assistance available [34]. Thus, the 3% FR case is considered as the underfilled case. Meanwhile, the 5% FR shows high thermal conductivity starting at 30 W and keeps increasing up to around 100 kW/(m K) as the heat input increases, which makes this filling ratio the optimum filling ratio for the working conditions of this research. The 10% and 15% FR cases show lower thermal conductivity for all heat input cases compared with the 5% FR case. Thus, they are considered as the overfilled conditions for this research. Figure 7(*b*) is a similar trend to Fig. 7(*a*), even though it can be seen that the 3% FR performed a little better in this case because of the inclination angle, 90 deg, such that the gravitational forces assist and speed the returning process of the condensate. Yet, the dry out happened at 150 W. Once again, the optimally filled condition, 5% FR, owns the highest thermal conductivity that is increasing as the heat input increases. Finally, the overfilled cases, 10%, and 15% FR showed lower thermal conductivity values under the same working conditions.

5.2 Effect of Inclination Angle

5.2.1 Effect of Inclination Angle on Thermal Resistance. The total thermal resistance of the heat pipe is calculated and plotted with regard to heat inputs for each filling ratio to clarify the impact of inclination angles on the thermal performance. Figures 8(*a*)–8(*d*) represent the four cases of the filling ratios, 3% FR, 5% FR, 10% FR, and 15% FR, respectively. From the basic understanding of the filling ratio and the conclusion drawn from the temperature distribution figures from the preceding paragraph, filling ratios used in this work can be denoted as underfilled which is the 3% FR, optimally filled is the 5% FR, and overfilled conditions are 10% FR and 15% FR. In Fig. 8(*a*) for the underfilled case, two working patterns were noticed, where for the small heat inputs, the thermal resistance was low; meanwhile, for all the cases after reaching medium to high heat inputs, the dry out conditions were dominant.

In Fig. 8(*a*), at 0 deg inclination, the thermal resistance recorded was 1.31 K/W for the case of 30 W (did not show up in the figures

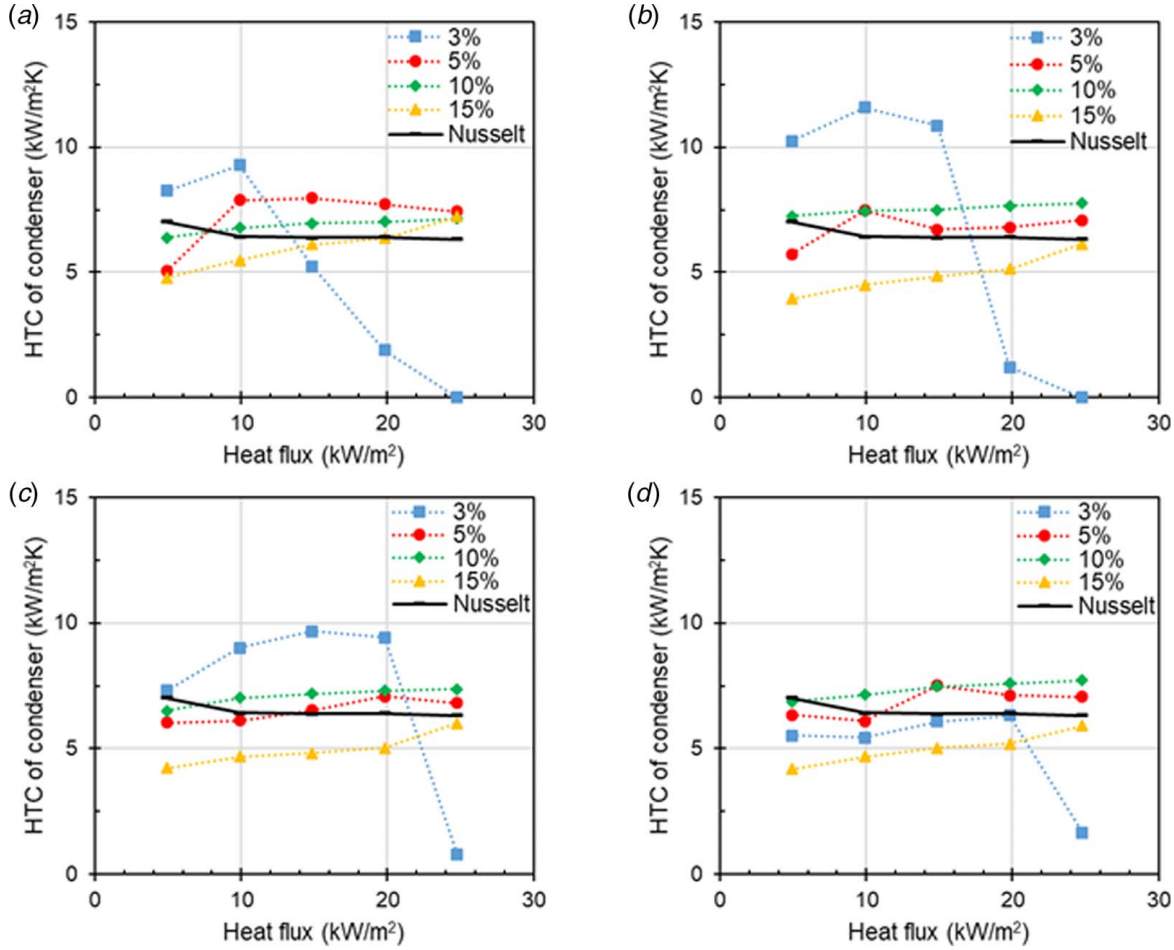

Fig. 6 Predicted and experimental HTC of condensation for different inclination angles: (*a*) 25 deg, (*b*) 55 deg, (*c*) 75 deg, and (*d*) 90 deg

because it is out of range) while for the higher heat inputs, all the cases experienced dry out conditions. This dry out related to the lack of working fluid in the evaporation section, the same problem faced Chen and Chou [11], where they had to terminate their tests because of the dry out conditions. Figure 8(*a*) shows that the best angle for the working cases was 55 deg. Furthermore, from Fig. 8(*a*), the other four heat input cases represented by 60 W, 90 W, 120 W, and 150 W followed the same pattern. A remarkably low thermal resistance was documented for low heat inputs. For high heat inputs, a dry out situation developed for the 25 deg, and 55 deg and high thermal resistance of 0.24 K/W noted for the 75 deg and 90 deg. The combination of working fluid content, evaporation rate, condensation rate, and gravity effect is the main reasons for such thermal behavior and results. As the working fluid amount is low, at high heat inputs, the evaporation rate will be higher, which means all the liquid at the evaporation section will evaporate before the condensate make it back to the evaporator. The same clarification was investigated and achieved numerically [17].

In Fig. 8(*b*), 5% FR, this figure shows the lowest thermal resistance levels compared with all other figures, encountering no dry out situation throughout all the heat input levels, which made it the optimum filling ratio case. The thermal resistance range for Fig. 8(*b*) is 0.019–0.028 K/W. Though it represents the optimal case, for 0 deg inclination, a poor thermal performance recorded as there is no gravity to extra assist in returning the condensate to the evaporation section. As the inclination angle increased, this issue has been resolved. There is a perfect combination of all factors mentioned before contributing to achieving the best performance. Meanwhile, the high effect of gravity at 90 deg may not be the best as it will drive an excessive amount of water back to the evaporation section, which will lead to pool boiling, thus lower thermal performance. It is seen from Fig. 8(*b*) that the 55 deg inclination case possessed the best thermal behavior compared with all other cases. From Fig. 8(*c*), it can be seen that heat pipes in the 55 deg inclination case perform the best in terms of thermal resistance. The most inferior thermal behavior was at the 0 deg inclination; this is due to the same reason for the optimal filling ratio case. At 0 deg inclination, the gravity effect is so small or neglected. Thus, the condensate will take a longer time to return to the evaporator; therefore, the evaporator's temperature would rise causing poor thermal behavior; similar conditions were numerically visualized by Alammar et al. [17]. The lowest thermal resistance achieved in this case was 0.032 K/W, which is higher than the highest thermal resistance in Fig. 8(*b*).

While for Fig. 8(*d*), we see a different story, the 0 deg inclination maintained the highest thermal performance for this filing ratio. This high thermal performance can be related to the liquid amount in the evaporation section. At low inclination (small or negligible gravity effect) and because of having a large amount of working fluid, the evaporator will be covered with a liquid layer, which will substantially augment the thermal performance. When the inclination angle increased, the liquid returning to the evaporation section increased. Thus, a liquid pool will be formed at the evaporation section which decreased the thermal performance of the heat pipe.

A similar conclusion was drawn experimentally and numerically, where the thermal behavior of a heat pipe is deprived due to the presence of a liquid pool in the evaporation section [18,35]. In summary, the different schemes of thermal behaviors encountered with each inclination angle showed that the orientation

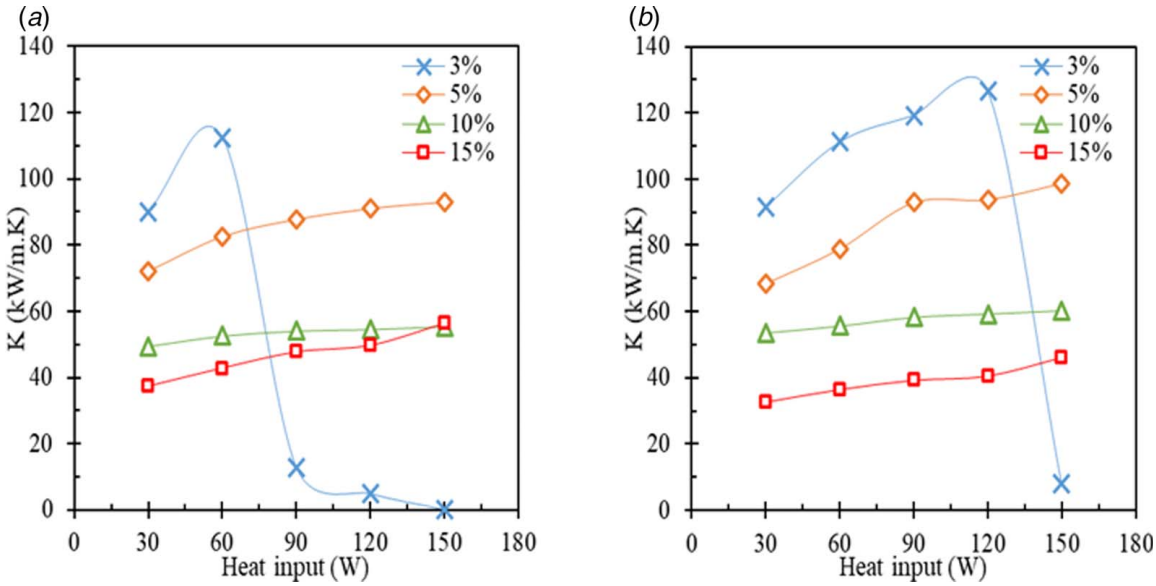

Fig. 7 Thermal conductivity for different heat inputs: (*a*) 25 deg inclination angle and (*b*) 90 deg inclination angle

(i.e., gravity effect) has a significant impact on the heat pipe's performance. The lowest thermal resistance achieved for this case was 0.028 K/W, which is equal to the highest thermal resistance in Fig. 8(*b*). Once again, Fig. 7 shows that the 5% FR represents the optimal case in terms of heat pipe thermal resistance.

Figure 9 represents a schematic illustration of the four filling ratio conditions inside the heat pipe. Again, all the explanations of enhancements mentioned earlier are observed in Figs. 9(*a*)–9(*d*). Starting with the underfilled working fluid conditions, Fig. 9(*a*), the lack of the working fluid inside the heat pipe can be noticed clearly. Hence, some local dry out zones will appear when the heat input increases due to the higher evaporation rate. Figure 9(*b*), which represents the optimum filling ratio, is always maintained a thin liquid film covering the evaporation section

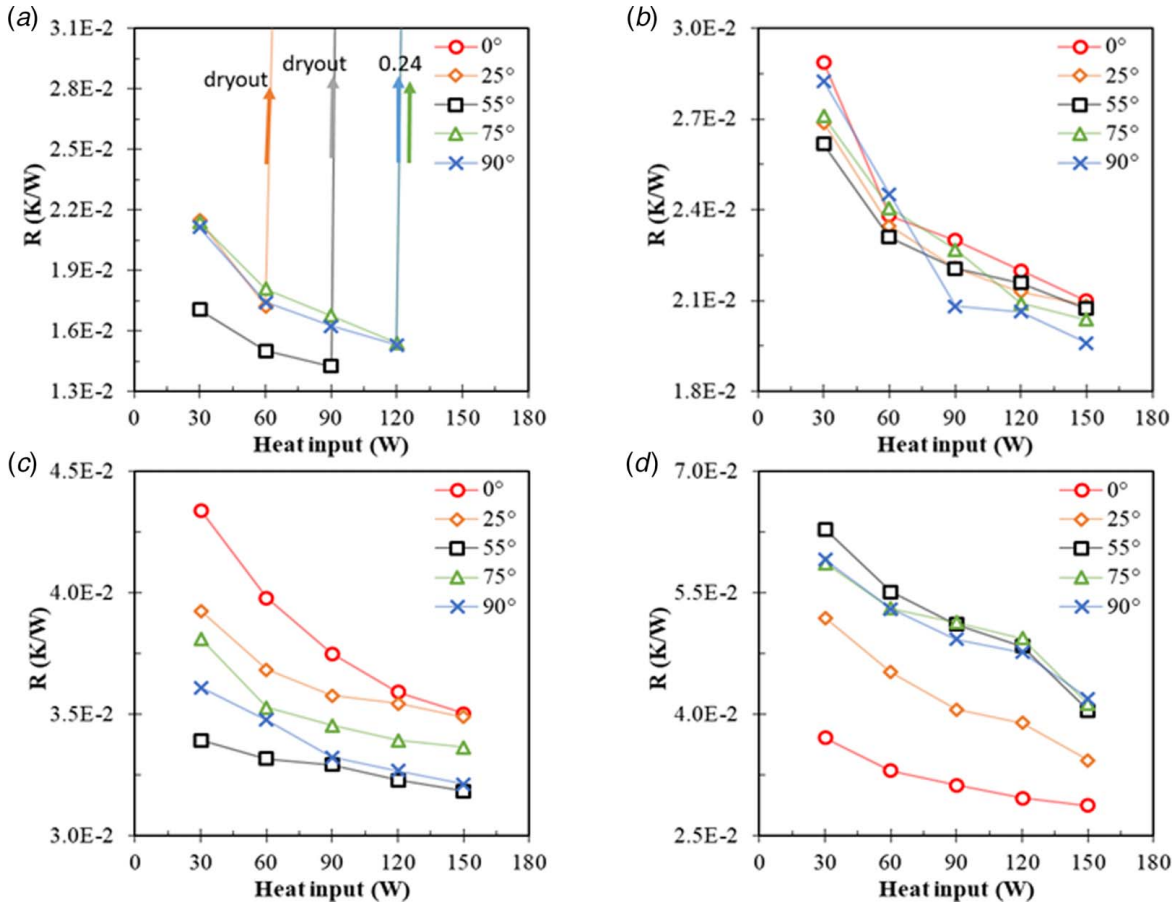

Fig. 8 Total thermal resistance with different heat inputs: (*a*) FR = 3%, (*b*) FR = 5%, (*c*) FR = 10%, and (*d*) FR = 15%

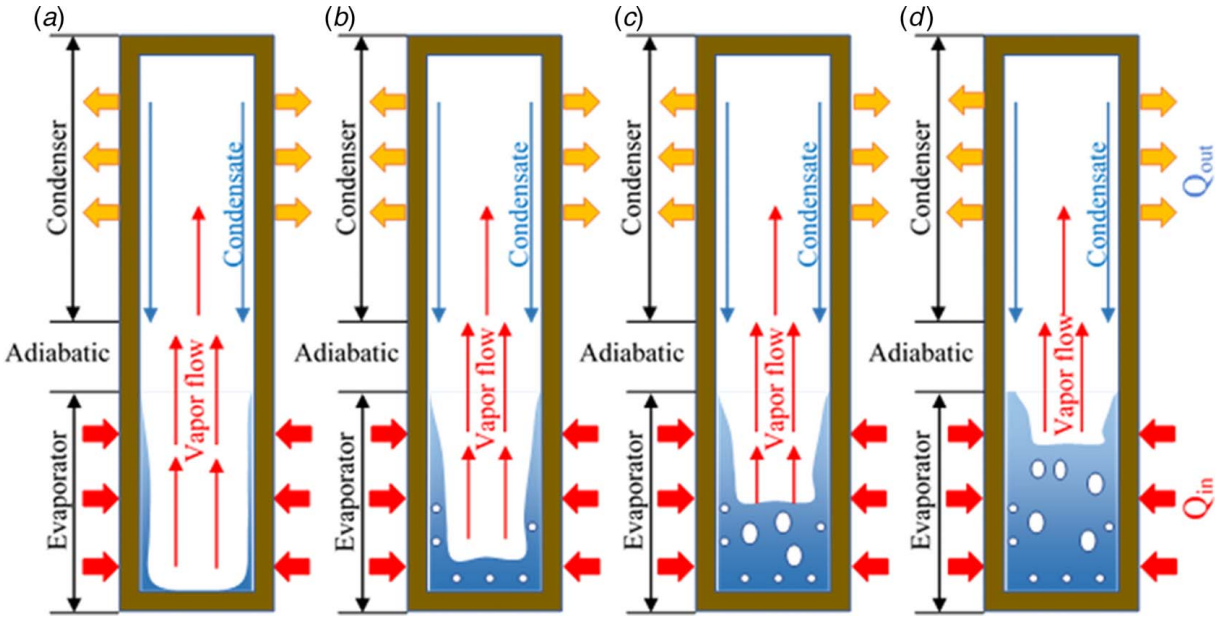

Fig. 9 Schematic illustrations of the heat pipe's filling ratio: (*a*) 3%, (*b*) 5%, (*c*) 10%, and (*d*) 15%

such that no dry out zones occurred; thin film evaporation was the dominant heat transfer mechanism. For Figs. 9(*c*) and 9(*d*), a liquid pool is formed at the evaporation section due to the excess amount of charged working fluid. No dry out issue for these two cases, but the pool boiling was the dominant heat transfer process, which is less effective compared with the thin film evaporation. In conclusion, Fig. 9 emphasizes and clarifies the effect and configuration of each filling ratio on the heat pipe performance.

6 Conclusions

An experimental investigation was carried out to optimize the filling ratio of heat pipes with nanoengineered evaporation sections. The effects of inclinations angle and heat loads were investigated in the steady-state conditions. The tests aimed at achieving the highest thermal performance represented by the lowest thermal resistance of the heat pipe. Copper heat pipe with an outer diameter of 12.7 mm and a length of 440 mm were used. Ultra-filtered de-ionized (DI) water was employed as the working fluid. Four different filling ratios were studied; 3%, 5%, 10%, and 15% FR, which is defined by the ratio of the working fluid volume to the volume of the evaporation section of the heat pipe. The results revealed that as the heat input increases, the temperature gradient among heat pipe ends increases. According to the obtained results, the filling ratios have been classified as an underfilled filling ratio (i.e., 3% FR), optimum filling ratio (i.e., 5% FR), and an overfilled filling ratio (i.e., 10% and 15% FR). In the underfilled conditions, dry out happened at high heat inputs. While in the overfilled cases, the presence of a liquid pool in the evaporation section affected the thermal performance negatively. The optimum filling ratio for this research was found to be 5% FR, at which a thin liquid film covered the evaporator walls under all testing conditions. Furthermore, the heat transfer capacity of the evaporation and condensation sections was characterized by the HTC for all filling ratios. The HTC results marked that the majority of the enhancement occurred in the evaporation section (evaporation HTC) compared with the condensation section (condensation HTC). Imura correlation, which is developed for the pool boiling heat transfer, was used to calculate the evaporation HTC theoretically. While for the condensation HTC, Nusselt correlation was used. The experimental enhancement in evaporation and condensation HTC was compared with a predicted one.

Acknowledgment

The authors would like to thank the Higher Committee for Education Development in Iraq (HCED) for providing the scholarship. This work is supported by the National Science Foundation (NSF) program of thermal transport processes under Grant No. 1336443 (Program Manager Dr. Jose Lage).

Conflict of Interest

There are no conflicts of interest.

Data Availability Statement

The authors attest that all data for this study are included in the paper.

Nomenclature

d = diameter
g = gravity
h = heat transfer coefficient
k = thermal conductivity
q = heat flux
A = area
I = current
L = length
P = power, pressure
Q = heat input
R = resistance
T = temperature
V = voltage
C_p = specific heat capacity
H_{fg} = latent heat of vaporization

Subscripts

a = air
amb = ambient
c = condenser section
c,i = inner wall temperature of condenser
c,th = condensation, theoretical

cop = copper
e = evaporation section
e,i = inner wall temperature of evaporator
e,th = evaporation, theoretical
eff = effective
f = working fluid
i = inner
ins = insulation
l = liquid
$loss$ = losses
o = outer
s = surface
$s1$ = insulation surface, location 1
$s2$ = insulation surface, location 2
sat = saturation
t = total
v = vapor

Greek Symbols

μ = dynamic viscosity
ρ = density
σ = uncertainty

References

[1] Yau, Y. H., and Ahmadzadehtalatapeh, M., 2010, "A Review on the Application of Horizontal Heat Pipe Heat Exchangers in Air Conditioning Systems in the Tropics," Appl. Therm. Eng., **30**(2–3), pp. 77–84.
[2] Guo, Z. J., Shao, J., Li, X. H., Liu, R. J., Wang, W., and Tian, X. L., 2016, "Application of Pump-Assisted Separate Heat Pipe on Dehumidifying Enhancement in Air Conditioning System," Appl. Therm. Eng., **98**, pp. 374–379.
[3] Yousefi, T., Mousavi, S. A., Farahbakhsh, B., and Saghir, M. Z., 2013, "Experimental Investigation on the Performance of CPU Coolers: Effect of Heat Pipe Inclination Angle and the Use of Nanofluids," Microelectr. Reliabil., **53**(12), pp. 1954–1961.
[4] Salman, A. S., Abdulrazzaq, N. M., Oudah, S. K., Tikadar, A., Anumbe, N., Paul, T. C., and Khan, J. A., 2019, "Experimental Investigation of the Impact of Geometrical Surface Modification on Spray Cooling Heat Transfer Performance in the Non-Boiling Regime," Int. J. Heat Mass Transfer, **133**, pp. 330–340.
[5] Nazari, M., Karami, M., and Ashouri, M., 2014, "Comparing the Thermal Performance of Water, Ethylene Glycol, Alumina and CNT Nanofluids in CPU Cooling: Experimental Study," Exp. Therm. Fluid Sci., **57**, pp. 371–377.
[6] Du, B., Hu, E., and Kolhe, M., 2013, "An Experimental Platform for Heat Pipe Solar Collector Testing," Renew. Sustain. Energy Rev., **17**, pp. 119–125.
[7] Jouhara, H., Szulgowska-Zgrzywa, M., Sayegh, M. A., Milko, J., Danielewicz, J., Nannou, T. K., and Lester, S. P., 2017, "The Performance of a Heat Pipe Based Solar PV/T Roof Collector and Its Potential Contribution in District Heating Applications," Energy, **136**, pp. 117–125.
[8] Noie, S. H., Sarmasti Emami, M. R., and Khoshnoodi, M., 2007, "Effect of Inclination Angle and Filling Ratio on Thermal Performance of a Two-Phase Closed Thermosyphon Under Normal Operating Conditions," Heat Transfer Eng., **28**(4), pp. 365–371.
[9] Lips, S., Lefèvre, F., and Bonjour, J., 2010, "Combined Effects of the Filling Ratio and the Vapour Space Thickness on the Performance of a Flat Plate Heat Pipe," Int. J. Heat Mass Transfer, **53**(4), pp. 694–702.
[10] Senthil, R., Ratchagaraja, D., Silambarasan, R., and Manikandan, R., 2016, "Contemplation of Thermal Characteristics by Filling Ratio of Al_2O_3 Nanofluid in Wire Mesh Heat Pipe," Alexandria Eng. J., **55**(2), pp. 1063–1068.
[11] Chen, J.-S., and Chou, J.-H., 2014, "Cooling Performance of Flat Plate Heat Pipes With Different Liquid Filling Ratios," Int. J. Heat Mass Transfer, **77**, pp. 874–882.
[12] Tharayil, T., Asirvatham, L. G., Ravindran, V., and Wongwises, S., 2016, "Effect of Filling Ratio on the Performance of a Novel Miniature Loop Heat Pipe Having Different Diameter Transport Lines," Appl. Therm. Eng., **106**, pp. 588–600.
[13] Sukchana, T., and Jaiboonma, C., 2013, "Effect of Filling Ratios and Adiabatic Length on Thermal Efficiency of Long Heat Pipe Filled With R-134a," Energy Procedia, **34**, pp. 298–306.
[14] Naresh, Y., and Balaji, C., 2017, "Experimental Investigations of Heat Transfer From an Internally Finned Two Phase Closed Thermosyphon," Appl. Therm. Eng., **112**, pp. 1658–1666.
[15] Xu, Z., Zhang, Y., Li, B., Wang, C.-C., and Ma, Q., 2018, "Heat Performances of a Thermosyphon as Affected by Evaporator Wettability and Filling Ratio," Appl. Therm. Eng., **129**, pp. 665–673.
[16] Lv, F. Y., Zhang, P., Orejon, D., Askounis, A., and Shen, B., 2017, "Heat Transfer Performance of a Lubricant-Infused Thermosyphon at Various Filling Ratios," Int. J. Heat Mass Transfer, **115**, pp. 725–736.
[17] Alammar, A. A., Al-Dadah, R. K., and Mahmoud, S. M., 2016, "Numerical Investigation of Effect of Fill Ratio and Inclination Angle on a Thermosiphon Heat Pipe Thermal Performance," Appl. Therm. Eng., **108**, pp. 1055–1065.
[18] Shabgard, H., Xiao, B., Faghri, A., Gupta, R., and Weissman, W., 2014, "Thermal Characteristics of a Closed Thermosyphon Under Various Filling Conditions," Int. J. Heat Mass Transfer, **70**, pp. 91–102.
[19] Aly, W. I. A., Elbalshouny, M. A., Abd El-Hameed, H. M., and Fatouh, M., 2017, "Thermal Performance Evaluation of a Helically-Micro-Grooved Heat Pipe Working With Water and Aqueous Al_2O_3 Nanofluid at Different Inclination Angle and Filling Ratio," Appl. Therm. Eng., **110**, pp. 1294–1304.
[20] Jafari, D., Di Marco, P., Filippeschi, S., and Franco, A., 2017, "An Experimental Investigation on the Evaporation and Condensation Heat Transfer of Two-Phase Closed Thermosyphons," Exp. Therm. Fluid Sci., **88**, pp. 111–123.
[21] Sarafraz, M. M., Hormozi, F., and Peyghambarzadeh, S. M., 2014, "Thermal Performance and Efficiency of a Thermosyphon Heat Pipe Working With a Biologically Ecofriendly Nanofluid," Int. Commun. Heat Mass Transfer, **57**, pp. 297–303.
[22] Abdulshaheed, A. A., Wang, P., Huang, G., and Li, C., 2019, "High Performance Copper-Water Heat Pipes With Nanoengineered Evaporator Sections," Int. J. Heat Mass Transfer, **133**, pp. 474–486.
[23] Enright, R., Miljkovic, N., Alvarado, J. L., Kim, K., and Rose, J. W., 2014, "Dropwise Condensation on Micro- and Nanostructured Surfaces," Nanoscale Microscale Thermophys. Eng., **18**(3), pp. 223–250.
[24] Cheng, J., Wang, G., Zhang, Y., Pi, P., and Xu, S., 2017, "Enhancement of Capillary and Thermal Performance of Grooved Copper Heat Pipe by Gradient Wettability Surface," Int. J. Heat Mass Transfer, **107**, pp. 586–591.
[25] Tang, Y., Hu, Z., Qing, J., Xie, Z., Fu, T., and Chen, W., 2013, "Experimental Investigation on Isothermal Performance of the Micro-Grooved Heat Pipe," Exp. Therm. Fluid Sci., **47**, pp. 143–149.
[26] Li, Y., Chen, S., He, B., Yan, Y., and Li, B., 2016, "Effects of Vacuuming Process Parameters on the Thermal Performance of Composite Heat Pipes," Appl. Therm. Eng., **99**, pp. 32–41.
[27] Imura, H., Kusuda, H., Ogata, J.-I., Miyazaki, T., and Sakamoto, N. J. J. T., 1979, "Heat Transfer in Two-Phase Closed-Type Thermosyphons," JSME Trans., **45**(393), pp. 712–722.
[28] Jafari, D., Filippeschi, S., Franco, A., and Di Marco, P., 2017, "Unsteady Experimental and Numerical Analysis of a Two-Phase Closed Thermosyphon at Different Filling Ratios," Exp. Therm. Fluid Sci., **81**, pp. 164–174.
[29] Hassan, H., and Harmand, S., 2017, "An Experimental Work on the Effect of the Radius of Rotation on the Performance of Revolving Heat Pipe (RVHP)," Appl. Therm. Eng., **123**, pp. 537–545.
[30] Chi, S. W., 1976, *Heat Pipe Theory and Practice*, Hemisphere Pub. Corp, Washington.
[31] Reay, D., McGlen, R., and Kew, P., 2013, *Heat Pipes: Theory, Design and Applications*, Butterworth-Heinemann.
[32] Ling, L., Zhang, Q., Yu, Y., Liao, S., and Sha, Z., 2016, "Experimental Study on the Thermal Characteristics of Micro Channel Separate Heat Pipe Respect to Different Filling Ratio," Appl. Therm. Eng., **102**, pp. 375–382.
[33] Lataoui, Z., and Jemni, A., 2017, "Experimental Investigation of a Stainless Steel Two-Phase Closed Thermosyphon," Appl. Therm. Eng., **121**, pp. 721–727.
[34] Byon, C., and Kim, S. J., 2012, "Capillary Performance of Bi-Porous Sintered Metal Wicks," Int. J. Heat Mass Transfer, **55**(15–16), pp. 4096–4103.
[35] Jafari, D., Filippeschi, S., Franco, A., and Di Marco, P., 2015, "Numerical Analysis of the Effect of Filling Ratio on the Transient Behaviour of a Two-Phase Closed Thermosyphon," Proceedings of the World Congress on Mechanical, Chemical, and Material Engineering, MCM 2015, Barcelona, Spain, July 20–21, Avestia Publishing.